Received: 9 February 2022 | Revised: 7 April 2022 | Accepted: 20 June 2022

DOI: 10.1002/ese3.1240

ORIGINAL ARTICLE

A novel hybrid solar chimney power plant: Performance analysis and deployment feasibility

Emad Abdelsalam[1] | **Fares Almomani**[2] | **Shadwa Ibrahim**[2]

[1]Energy Engineering Department, Al Hussein Technical University, Amman, Jordan

[2]Department of Chemical Engineering, College of Engineering, Qatar University, Doha, Qatar

Correspondence
Fares Almomani, Chemical Engineering Department, Qatar University, Doha, Qatar.
Email: Falmomani@qu.edu.qa

Abstract

This study presents a novel hybrid solar chimney power plant (HSCPP) design. The HSCPP preserves the typical solar chimney power plant (SCPP), with an additional seawater pool at the base and water sprinklers at the top. This new and novel design configuration offers an opportunity to run the system during the daytime as a traditional SCPP and as a downdraft cooling tower at night. The performance of the HSCPP was analyzed in 16 cities in the Kingdom of Saudi Arabia (KSA) that span the entire geographical area of the country to select the optimal location for installation. The results showed that the highest annual electrical energy production of 676.20 MWh was achieved in the southern city of Shahrurah. However, the lowest annual electrical energy production of 347.59 MWh was found at Wajh, in the west. The highest annual freshwater production was 143,898 tons at Riyadh, in the center. However, the lowest annual freshwater production was 77,868 tons at Muwayh, in the west. Furthermore, the results showed that the proposed HSCPP increased electrical power production by 55% and freshwater production by 20% when compared to traditional SCPP. In addition, an outstanding reduction in CO_2 emissions by approximately 56% was associated with such an application of HSCPP. The performance of the HSCPP is very promising, however, the geographical location to install the HSCPP is performance-critical. Hence, the optimal locations were found to be from the center to the southern part of the KSA.

KEYWORDS

energy efficiency, power generation, power management, solar energy

1 | INTRODUCTION

1.1 | Background

The need for energy and clean water resources will exponentially expand in the next years to keep up with rising lifestyle standards, worldwide economic growth, and population growth.[1,2] Fossil fuels (oil, natural gas, and coal) have proven to be effective drivers to support the global energy demand. However, their burning was always regarded as one of the causes of the global warming (GW) problem by raising the concentration of CO_2 and other greenhouse gasses (GHGs) in the atmosphere.[3,4] Chemical substances in the flue gases, in

general, contribute to air pollution that has a direct impact on human health,[5,6] the Environment,[7] and communities' welfare. As a result, scientific research into novel alternatives to conventional energy resources is required.

Renewable and clean energy resources that are continually replenished by nature could satisfy part of the global energy demand without any GHGs emissions.[8] As a result, various countries have invested in renewable energy resources in the hope to cover the global energy needs.[9] It was reported that electricity generation from renewable resources increased by more than 8% to reach 8 300 TWh in 2021, representing the fastest year-on-year growth since the 1970s. Furthermore, governments all over the world were concerned with developing regulations and policies to support such scientific efforts and to ensure that the use of these clean energy resources is facilitated.[10]

The diversity of renewable energy technologies and resources is one of its most notable characteristics. Different studies believe that the ultimate size of the renewable energy resource is large to the limit that they could make a very significant contribution to global energy demands.[11] Solar energy,[12] wind,[13] hydropower[14] biomass,[4,13,15] and geothermal are among the leading and most developed renewable resources and technologies. Renewables such as solar, modern biomass and wind power contribute to around 3% of electricity and 2% of primary energy. Although these technologies offer large potential for growth and significant environmental benefits, their economic aspect still requires further investigation to ensure high performance within an acceptable range of localized cost of energy (LCOE).[16]

Solar energy, in specific, is amongst the most promising renewable energy resource with low GHGs emissions.[17] Solar energy has the potential to be converted into thermal energy, which can then be used to heat a building or water, or it can be converted into electricity via solar photovoltaic (PV) cells[18] or concentrating solar power (CSP) systems. The CSP technologies generate electricity by concentrating direct-beam solar irradiance to heat a liquid, solid, or gas, which is then used to generate electricity in a downstream process. These technologies are technically well proven with numerous systems installed around the world over the last few decades.[19,20]

Solar chimney (SC) is regarded as an outstanding power generating plant due to its simple design (no mechanical parts, low maintenance, and no electrical consumption), very low environmental impact (no GW effects or pollution) and dual cation (can be used for both heating and cooling).[16,17,21] The first pilot study of the SC power plant was initiated in Spain during the 1980s.[17,22] The electricity generated from the first innovative and optimized design of the solar chimney power plant (SCPP) was in the range of 100–200 MW.[23] Recent research work on the SCCP technologies focused on (1) developing an accurate mathematical model to optimize the process, (2) proposing system modification, or (3) adding new elements to the SC structure or combining it with other technology (i.e., hybrid systems). These efforts are aimed at improving the SCPP design and feasibility, enhancing the efficiency and performance while reducing the cost, increasing the power production and at a certain time producing additional products (e.g., desalinated water). Another important aspect that was intensively explored was the SC configuration and geometrical parameters to enhance power generation. Works on the constructal configuration of SC was varied and based on experimental studies,[24,25] process simulation,[26,27] optimization,[28] and numerical calculations.[29,30] As an example, Zhou et al.[31] presented in 2010 a review that explains the progress in SC throughout the years 1982 to 2010 from theoretical to pilot-plant operation. Fathi et al.[32] showed that the productivity of SCPP could be increased by utilizing waste heat from power plants. The effect of the design geometry on the performance of the SCPP was discussed by Maia et al.[33] Mathur[34] studied the effect of the inclination of the collector on the performance of SCPP and concluded that the optimum inclination varies from 40° to 60° depending upon the latitude of the place. Ming et al.[35] showed that structure of the SC plyas an important role in power generation and the corresponding efficiencies. Larbi et al.[36] performed a performance analysis of an SCPP in the southwestern region of Algeria to identify the most important performance parameters. Solar radiation, ambient temperature, chimney height and the surface of the collector were identified as the main efficiency parameters that might significantly affect the system performance. Guo et al.[37] showed through numerical simulation that the SCPP can produce up to 120 kW when the solar radiation is around 600 W/m^2. Pasumarthi and Sherif[38] developed a mathematical model to help analyze the factors that might influence the system's performance. Kiwan and Salam[39] modified the design of the SCPP by adding water pool in the base. The modified design has high solar utilization capacity and successfully produces energy and desalinated water. Abdelmohimen and Algarni[40] showed that a SCPP with a chimney hight of 194 and collector dimeter of 244 m is capable of generating an average of 56 kW/month in the city of Riyadh. Chergui et al.[41] conducted a heat transfer and airflow modeling analysis of the SCPP to investigate the effect of airflow velocity and temperature distribution on system performance. The developed model aided the

SC designer in accurately locating the mechanical conversion device within the collector chimney system. Xu and Zhou[42] developed a mathematical model that investigate the operation of the SCPP within an agricultural area. It was concluded that the agricultural benefits compensate for the decrease in electricity production. Khan et al.[43] presented a comprehensive review that outlines the benefits of coupling SCPP with reverse osmosis for water desalination. Similarly, Zuo et al.[44] presented a comprehensive study on the use of wind supercharged SCPP for seawater desalination. Other works that incorporated power plant with desalination processes were presented elsewhere.[45,46] Asnaghi and Ladjevardi[47] showed that the SCPP can be impliminted off-grid to provide electricity to urban areas if the land is available. New structures consisting of SCPP and building ventilation were presented by Harris and Helwig.[48] Zandian and Ashjaee[49] performed research work about ventilation and its relation to the airflow inside the roof SC. Arce et al.[50] studied the thermal performance of a SC for natural ventilation. The results reveal that maximum irradiation of 604 W/m^2 can create a maximum air temperature difference of 7°C. Afonso and Oliveira[51] presented interesting results that prove the feasibility of using SC for buildings' natural ventilation to improve indoor air quality. The impact of changing the configuration of the SCPP-single or multiple turbines- on the power generation, power conversion unit (PCU), energy yield, and efficiency was discussed by Afonso and Oliveira[51] and Fluri and Von[52]. Furthermore, the utilization of different types of Basement,[53,54] collectors,[55,56] and absorber materials[57] was illustrated. Combining with other systems or proposing various modifications to the SCPP was the concern of the majority of experimental and numerical work executed on SCPP. Klimes et al.[58] compared the energy conversion efficiency from SCPP with solar PV-powered fans. The PV-powered fans significantly outperform the SCPP in terms of converting solar energy into kinetic energy. Kommalapati et al.[59] showed that using the SCPP can reduce the GHGs emissions from the power plant by 55%. Other studies integrate SCPP with PV systems to achieve seawater desalination under practical weather conditions. Two designs were suggested to increase the performance of the process by taking into account the income from the generation of electricity and the production of freshwater. The first design combine the PV system with SCPP, while the second and focused on modifying the SCPP design and configuration itself.[39,60] For the PV-SCPP system PV water pool installed in the base of the SC allow to cool down the PV and increase efficiency. This system offered the the generation of fresh water and electricity. The other system focused on developing a steady state movement of air in the system to enhance desalinated water production. Insulating the collector's surface is another important design to highlight. Insulating the collectors showed a significant improvement in the system efficiency and power outcome.[61] Integrating SC with wind capturing in another advanced technique used to increase the process performance. The wind capturing device capture energy from wind at an elevated height and contribute to the system energy production. Tavakolinia[62] presented a study where the wind-catcher improve natural ventilation system to building in the Los Angles area. The system offers a way to redeuce pollution, under low energy requirements without any significant noise compared to traditional air conditioning systems. Prima and Prima[63] presented similar results of applying the concept of the wind-catcher combined with SC on a humid climate. The SC was also combined with wind turbine to provide a hybrid system that can generate electricity. Zandian and Ashjaee[49] showed that the SCPP can be used in power plant's not onlty to enhance thermal efficiency but also to provide cooling facility by acting as a cooling tower (CT). Ming et al.[64] suggested that the SCPP can be upgraded adding a nozzle for hot water inside the collector.

Although the applications of the SCPP showed promise in terms of energy security, some challenges must be overcome to allow stable large-scale implementation. For an instant, the requirement for high chimneys and big areas of land, low LCOE, and low thermal efficiency are issues that required further investigation. The aforementioned literature review has underlined the significance of developing innovative designs of the SCPP to achieve the desired improvement. Moreover, limited published articles were involved in integrating CT with the SCPP. Therefore, this study presents a remarkable hybrid solar chimney power plant (HSCPP) design that combined CT with SCPP to produce electricity and desalinated water. The proposed design benefits from using a bidirectional turbine to operate the SC structure as a power plant in the daytime and as CT at nighttime, achieving continuous system operation. Previously, this design was tested in the city of Aqaba, Jordan, and showed impressive results.[67] However, as the weather conditions (e.g., temperature, solar radiation intensity, and humidity) and the geographical location have a high impact on the system operation HSCPP required further investigation.

1.2 | Goals and objectives

This study focused on assessing the performance of the HSCPP under different climate conditions and diverse

geographical areas of Kingdom of Saudi Arabia (KSA). Although the performance of the traditional SCPP was previously investigated in five cities of KSA,[42] this will be the first study the explore the operation of the new HSCPP design in different cities. The new design offer dual action that generates electricity, desalinated water and cooling water. Therefore, the new design can be used in/off-grid to provide energy and water as well as in industrial institutions. The design was tested in a wider geographical area of 16 cities to select the best locations for higher productivity of the HSCPP. The work aims also to present the superior performance of the new proposed design over the traditional SCPP design, assess the performance in each city, correlate the productivity (electricity and water) and performance to weather data, and select the optimal locations for water and electricity production.

2 | MATERIALS AND METHODS

2.1 | HSCPP description

2.1.1 | System structure

The HSCPP system combines the working principles and technologies of both a traditional SCPP and a CT. As shown in Figure 1, the HSCPP system consists of a SC (height = 200 m and diameter = 10 m), a collector (diameter = 250 m), and a bidirectional turbine. The HSCPP is equipped with a seawater pool (diameter = 30 m) at the base of the collector. The height of the collector starts at 6 m at the entrance and gradually increases to 12 m at the chimney base. All physical dimensions and components are shown in Figure 1A,B. The turbine is located at the bottom of the chimney and above the ground. Gutters are installed at the inner walls of the chimney and connected to pipes to escort the collected desalinated water to a reservoir outside the chimney. The top section of the chimney is fitted with water sprinklers. Water is pumped using an external pump from a reservoir outside the chimney. The seawater pool is centralized under the chimney and fitted with water pipes to bring in the water from an outside reservoir. The chimney and the base are assumed to be made of concrete. The rooftop of the collector is made of glass. The turbine is bidirectional to allow energy harvesting in both directions.

2.1.2 | System modes of operations

The HSCPP is configured to run in two mutually exclusive modes: conventional SCPP mode and CT mode.

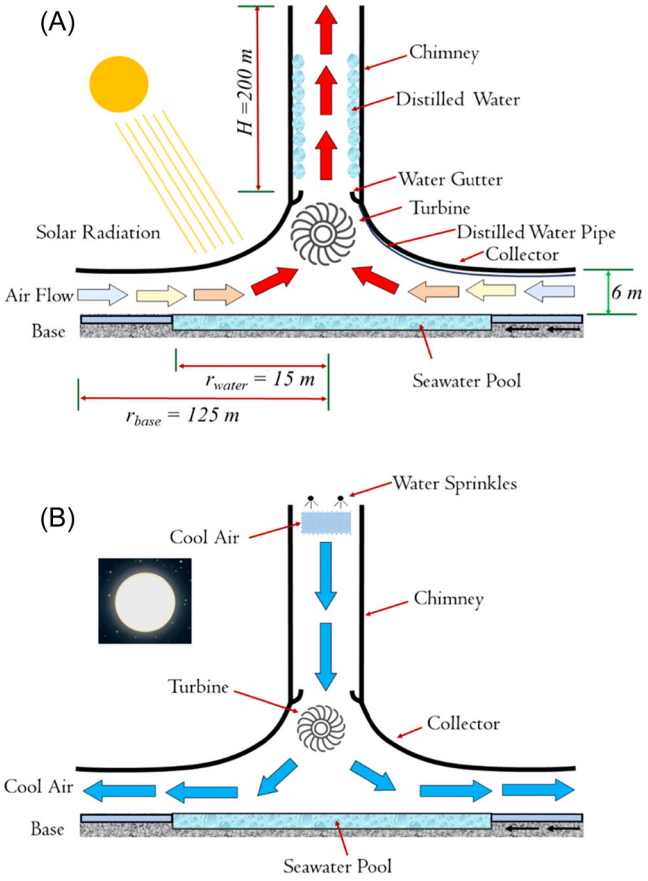

FIGURE 1 Schematic operation with physical dimensions of the proposed hybrid solar chimney power plant system (A) working as solar chimney power plant, and (B) working as cooling tower

The principle of operation of both modes is the density difference between the air inside the system and the ambient air. Furthermore, the heat flow direction of the air in the system is the main difference in both modes. The principal operation of both modes is explained in the next section.

SCPP mode

Figure 1A presents the operation of the structure as SCPP. Solar irradiation intercepted at the surface of the collector heats the air under the collector and increases its temperature and decreases its density. Therefore, the kinetic velocity of air increase along the sloped roof. This allows the air under the collector to expand while flowing from sector one to two over the seawater pool. As the air moves over the seawater pool, it becomes humid due to the bouncy effect at the seawater pool. With the increase in the solar intensity during the day, the air temperature under the collector increases exponentially and continues to expand over the seawater pool at the bottom of the structure. This develops a differential pressure between the bottom and the top of the SCPP and

pushes the hot and humid air upward to the top of the chimney. While moving upward, the temperature of humid air decrease leading to water desalination at the inner walls of the chimney. As the hot air moves up the chimney it interacts with the turbine to produce electricity. The temperature difference between the air inside and outside the chimney determines the velocity of the air ascending through the chimney, as presented by Equation (23). Then, the air leaves the chimney to the surrounding area. The direction of the airflow throughout the different sectors of the system (entrance, collector, seawater pool, turbine, and chimney) is presented in Figure 1A. The color of the arrows indicates the temperature increase of the air as it flows through the system. As the temperature and solar irradiation increase during the day, it is expected that the production of desalinated water and electricity increases to reach a maximum around noon time. The production declines in the afternoon due to a decline in the temperature and solar irradiation and ceases at sunset. The operation of the SCPP is highly dependent on solar irradiation, hence, it only operates in the daytime.

CT mode

The system components that are needed to operate during the CT mode are the chimney, turbine, and water sprinklers, as shown in Figure 1B. The CT operates during the nighttime as it does not need solar irradiation. The operation as a CT starts by spraying a mist of cool water on the hot and dry air located at the top of the chimney, as shown in Figure 1B. The sprayed water evaporates almost instantly to be absorbed by the hot air. This decreases the air temperature and increases its density. As a result, and according to the ideal gas law, an increase in pressure occurs at the top of the chimney leading to accelerating the air toward the bottom of the chimney. Like the SCPP mode, the temperature difference between the air inside and outside the chimney determines the velocity of the air ascending the chimney, Equation (23). As the air descends it interacts with the turbine to produce electricity, and then exits the chimney to the collector area. The direction of the arrows in Figure 1B shows the direction of the airflow during this mode. The operation of the CT mode is very dependent on the temperature and humidity of the ambient air. This will be addressed in detail in the results and discussion section.

The transfer between SCPP and CT modes is done by the bidirectional turbine that changes its spinning direction (clockwise or counterclockwise) based on the airflow. Therefore, the HSCPP functions as SCPP during the day and as CT at night. Hence, the HSCPP potentially offers continuous generation of electricity and desalinated water if the weather conditions permit. This resulted in higher system utilization and efficiency compared to the traditional SCPP design, in addition to a rapid decrease in the LCOE.

2.2 | Mathematical model

The mass and energy balance of the novel design was established using the equations that are listed in this section, and as shown in Figure 2A. A mathematical model was developed for each sector of the SCPP using MATLAB software and solved numerically. The mathematical model contains equations corresponding to Sector 1 (solar air heating), Sector 2 (air humidification), and Sector 3 (water desalination and power productions). The

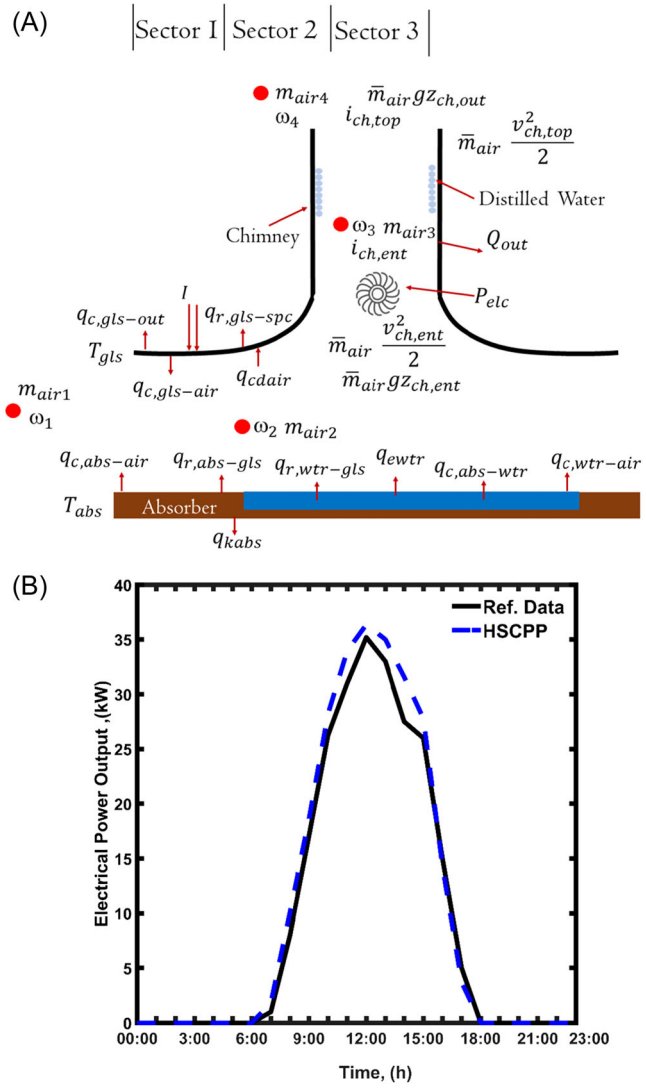

FIGURE 2 Diagram represents (A) the energy balance equations: showing sector 1, sector 2, and sector 3 of the hybrid solar chimney power plant, (B) validation results

hourly weather data (solar irradiation, wind velocity, temperature, and relative humidity) were obtained for each city (8760 h/year) and used to solve the mathematical model basis. The model reads the four input weather parameters and calculates the temperature of the collector roof, base, and the air under the collector using Matlab genetic algorithm. The program iterates to calculate all parameters and converges when the error is less than 10^{-6}. The model first calculates the temperature profile of the air in Sector 1 every 5 m starting from the entrance of the collector and ending at the edge of the seawater pool. Next, the program calculates the amount of humidification, enthalpy, and the temperature of the air over the sweater pool. Last, the model calculates the air velocity, mass air flow, electrical power generated, and the amount of water desalination in the last sector (chimney). The mathematical model was validated against a well-known baseline prototype built by Arce et al.[52] and Afonso and Oliveira.53

The following section depicts the energy balance equations for the various sectors of the HSCPP. The objective of the model was to calculate the temperature of the air at all three sectors and then combine the results to find the temperature profile for the entire system. However, The model's detailed equations can be found in the supplemental material of our previous publications.[67,68] The energy balance was performed in the following sections:

2.2.1 | Sector 1: Solar air heating

Airflow:

The rate at which the air temperature changes with distance as a function of the convective heat transfer rates between the glass of the collector and air, and the absorber and air, was applied as follows:

$$q_{c,gls-air} + q_{c,abs-air} = -\frac{c_{p,air}\dot{m}_{air}}{2\pi r}\frac{dT_{air}}{dr}, \quad (1)$$

where $\omega_1 = \omega_2$, from air mass balance equation.

The energy balance equations at the absorber and collector as related to the solar irradiations were applied as follows:

Absorber:

$$q_{r,abs-gls} + q_{c,abs-air} + q_{kabs} = \alpha_{abs}\tau_{gls}I. \quad (2)$$

Collector:

$$q_{c,gls-out} + q_{c,gls-air} + q_{r,gls-spc} = \alpha_{gls}I + q_{r,abs-gls}. \quad (3)$$

Collector to air convective heat transfer rate was applied as follows:

$$q_{c,gls-air} = h_{c,gls-air}(T_{gls} - T_{air}). \quad (4)$$

Base to air convective heat transfer rate was applied as follows:

$$q_{c,abs-air} = h_{c,abs-air}(T_{abs} - T_{air}). \quad (5)$$

The radiative heat transfer rate established between the absorber and the solar collector was determined using the below equation:

$$q_{r,abs-gls} = h_{r,abs-gls}(T_{abs} - T_{gls}). \quad (6)$$

Convective heat transfer rate between the collector and outside environment was determined using the below equation:

$$q_{c,gls-spc} = h_{c,gls-spc}(T_{gls} - T_{spc}). \quad (7)$$

The convective heat transfer coefficient ($h_{c,gls-spc}$) was applied as follows:

$$h_{c,gls-spc} = 2.8 + 3.0v_0, \quad (8)$$

where, v_0 is the horizontal wind speed just above the collector. The temperature of the sky was applied as follows:

$$T_{spc} = T_{out} - 6. \quad (9)$$

Collector to outside environment radiation heat transfer rate was applied as follows:

$$q_{r,gls-spc} = h_{r,gls-spc}(T_{gls} - T_{spc}). \quad (10)$$

2.2.2 | Sector 2: Air humidification

Similarly, the rate at which the air temperature changes with distance, over the seawater pool, as a function of the convective heat transfer rates between the water and air, and the glass and air, was applied as follows:

$$q_{c,gls-air} + q_{c,wtr-air} = -\frac{c_{p,air}\dot{m}_{air}}{2\pi r}\frac{dT_{air}}{dr}. \quad (11)$$

The convective heat transfer rate between the absorber and water was determined using the below equation:

$$q_{c,abs-wtr} + q_{kabs} = \alpha_{gls}\tau_{wtr}\tau_{gls}I. \quad (12)$$

The radiative heat transfer rate between the water and glass was as follows:

$$q_{r,gls-spc} + q_{c,gls-out} = q_{c,gls-air} + q_{r,wtr-gls} + \alpha_{gls} I. \tag{13}$$

The energy balance of water per unit area of the chimney was calculated using the following equation:

$$q_{ewtr} + q_{r,wtr-air} + q_{c,wtr-air} + \frac{c_{p,wtr}\bar{m}_{wtr}}{2\pi r}\frac{dT_{wtr}}{dr} = q_{c,abs-wtr} + \alpha_{wtr}\tau_{gls} I. \tag{14}$$

2.2.3 | Sector 3: Water desalination and power productions

To calculate the electrical power and desalinated power generated while the HSCPP was operating using the SCPP mode, the following energy balance equations were applied:

$$P_{elc} + Q_{out} = \overline{m}_{air}\left[\left(\frac{v_{ch,ent}^2}{2} + gz_{ch,ent} + i_{ch,ent}\right) - \left(\frac{v_{ch,out}^2}{2} + gz_{ch,out} + i_{ch,out}\right)\right]. \tag{15}$$

where,

$$Q_{out} = \overline{m}_{air}[(i_{ch,ent} - i_{ch,out}) - (\omega_4 - \omega_3) i_{wtr}]. \tag{16}$$

The rate of water condensation at the inner walls of the chimney was determined using the below equation:

$$\overline{m}_{wtr} = \overline{m}_{air}(\omega_4 - \omega_3). \tag{17}$$

The enthalpy[56] of the moist air entering the chimney ($i_{ch,ent}$) was calculated as follows:

$$i_{ch,ent} = T_{air} + \omega_3(2501.3 + 1.86T_{air}). \tag{18}$$

Equation (18) was also used to calculate the enthalpy of the air that enters the chimney when the HSCPP was running the CT mode.

The enthalpy of the air after cooling can be calculated as follows:

$$i_{vap} = i_{air} + \omega_{vap} i_{wtr}. \tag{19}$$

The enthalpies of the air and water were calculated as below:

$$i_{air} = c_{p,air} T_o, \tag{20}$$

$$i_{wtr} = c_{p,wtr} T_{wtr}. \tag{21}$$

The temperature of the produced vapor was calculated as follows:

$$c_{p,air} T_o + (\omega_{air} 2501.3 + T_o 1.86) = (\omega_{vap} 2501.3 + T_{vap} 1.86) + c_{p,air} T_{vap}. \tag{22}$$

The velocity of the air at the entrance of the chimney was determined using the below equation[57]:

$$V_{ch} = \sqrt{2gH_{ch}\frac{T_{ch,ent} - T_{out}}{T_{out}}}. \tag{23}$$

The output power produced by the turbine was calculated as follows[57]:

$$P_{elc} = \frac{1}{2}\rho_{en,ch} C_f A_{ch} V_{ch}^3. \tag{24}$$

Where, C_f is the turbine efficiency, 0.42.

3 | RESULTS AND DISCUSSION

The operation and performance of the HSCPP depend on the weather conditions. Hence, geographical location plays a vital role in selecting the optimal location for the deployment of the HSCPP. Due to the vast area of the KSA, weather variations from one location to another are very possible. Hence, to study the impact of location and weather conditions on the performance of the HSCPP, the area of the KSA was partitioned into several segments. Figure 3 shows the map of the KSA highlighted in five different colors representing five different segments: north, south, east, west, and center. Sixteen cities were selected to represent the segments as shown in Table 1.

3.1 | Organization of this section

In the upcoming discussion, the data collected from the 16 cities will be presented in different manners to allow for a complete analysis of the performance of the proposed design of HSCPP. The available data includes the weather conditions of the selected cities, along with

the electricity and water production. Various types of figures were plotted, based on the collected and generated data, focusing on different performance measures of the HSCPP for each location. First, two figures will illustrate an example of weather data variation during the day in one of the cities (e.g., Qaisumah) of KSA on the 17th of July. The first figure presents the weather data profile, while the second one presents solar irradiation as well as electricity and water production. Next, a comparison based on the hourly average solar irradiation between five cities, which represent the five geographical areas will be represented. Then, the hourly average solar irradiation over the entire year will be represented for all cities allowing the desired comparison between them. After that, an example of the hourly average ambient temperature of the same five cities will be shown. Next, an arrangement for the timeline of the year will be conducted and applied to the values of wind speed, electrical energy production, and water production. Finally, a table with the annual electrical energy production and desalinated water production for each city will be discussed.

3.2 | Selected examples of weather profiles and performance figures

Figure 4 represents the solar irradiation and the weather conditions on the 17th of July, in the city of Qaisumah. Solar irradiation values started to increase almost after 05:00 until approximately 09:00. Then, minimal fluctuations were observed in solar irradiation values, until reaching the highest value of the day, which was 792 W/m^2 at 14:00. After that, the solar irradiation value decreased dramatically until reaching almost zero at 18:00. The case is different for the humidity, as the highest values of almost 19% were observed at the beginning of the day (between 04:00 and 05:00). The humidity decreased slightly in the middle of the day reaching the lowest value of 9% and then increased at nighttime. Temperatures values varied between 31°C at

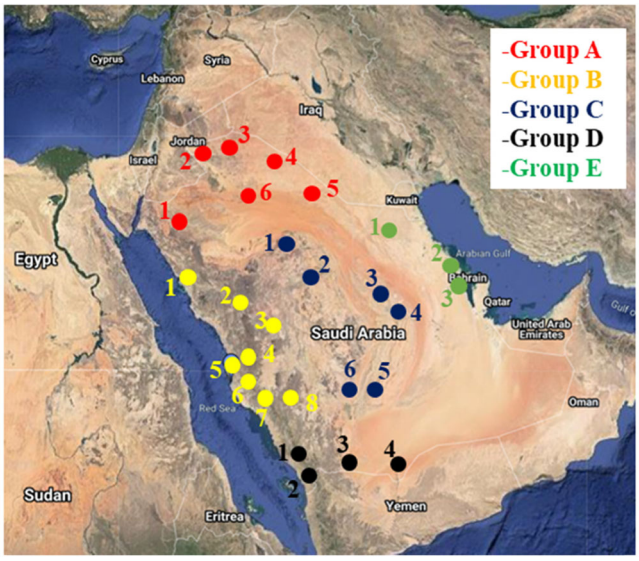

FIGURE 3 Geographical grouping of selected cities for the deployment of the hybrid solar chimney power plant in Kingdom of Saudi Arabia

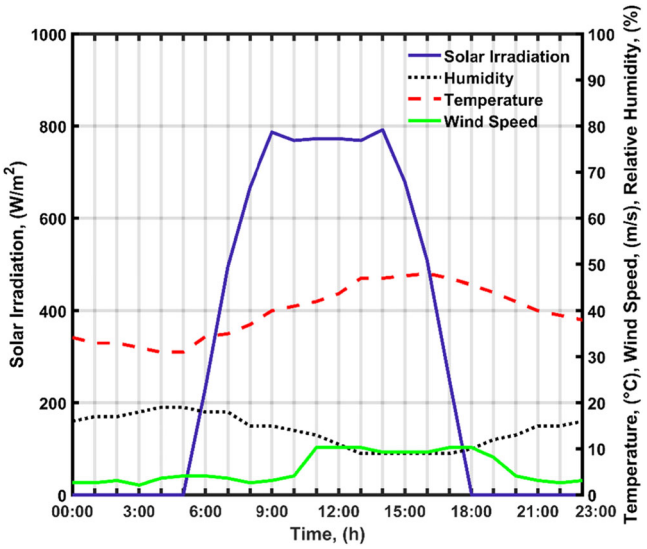

FIGURE 4 Solar irradiation and the weather conditions on 17th of July in Qaisumah, Kingdom of Saudi Arabia

Group A (north, red)	Group B (west, yellow)	Group C (center, blue)	Group D (south, black)	Group E (east, green)
Rafha	Bisha	Hail	Najran	Qaisumah
Sakakah	Jeddah	Wadi Dawasir	Jizan	Dhahran
Tabuk	Muwayh	Riyadh	Shahrurah	
Turaif	Wajh			

TABLE 1 Selected cities within the different geographical areas to operate the hybrid solar chimney power plant

04:00 and 05:00 and 48°C at 16:00 throughout the day, showing the highest values in the middle of the day. Since the CT performance is affected by the temperature and the air humidity, it is expected that the lowest electrical energy production will be in the hours of 04:00 and/or 05:00. That is because they have the lowest temperatures and the highest humidity values. The case for the SC performance will be slightly different as it is affected mainly by the solar irradiation and temperature and the lowest values for the electrical energy production will be expected to be at the two ends of the operation timeline, where the solar irradiation is the lowest. For the wind speed, values were found to be between 2.1 and 10.3 m/s, and the highest values were approximately observed between 17:00 and 18:00. It should be said that it will be expected for the highest water production value to be approximately in the middle of the day. That is because it is affected by ambient temperature, solar irradiation, and wind speed. The ambient temperature and the solar irradiation, affect the temperature under the collector. Therefore, It is expected that whenever the values of these parameters are the highest, the water production will be high. High temperature and solar irradiation will contribute to more water evaporation from the seawater pool. In addition, water production is directly proportional to wind speed.

Figure 5 presents the solar irradiation, and the electrical and water production on the 17th of July in Qaisumah. The electrical energy can be produced at nighttime using the CT mode and at daytime using the SCPP mode. Noticeably, while ignoring the slight fluctuations in the middle of the day, the trend line of the electrical energy at the daytime seems to imitate the solar irradiation trend line. The production of electrical energy in the daytime is directly dependent on solar irradiation. On the other hand, the trend of the electrical energy production at nighttime sounds to have a much more stable behavior with only 10.7 kWh difference between the highest and lowest values. That is because during the operation as CT the system ensures that the air is saturated with the sprayed water. The lowest electrical energy during the operation as CT was found to occur between 04:00 and 05:00 with a value of 156.7 kWh. The lowest electrical energy production value during the operation as conventional SCPP was found to be at the second end of the operation timeline, specifically at 17:00 with a value of 15.7 kWh. It can be observed that the highest electrical energy production value occurs when the system was operated as CT, specifically at 19:00 with a value of 167.4 kWh, while the lowest value was observed at the operation as SCPP, precisely at 17:00 with a value of 15.7 kWh. It can be approximated that these two values represent the last value in the operation of as SCPP and the first value of the operation as CT, respectively. In other words, the increase in the electrical energy production values is due to the switch of the operation between the SCPP and CT. Moreover, the highest and lowest water production values were found to be at noon (71.3 tons) and 06:00 (11.1 tons), respectively.

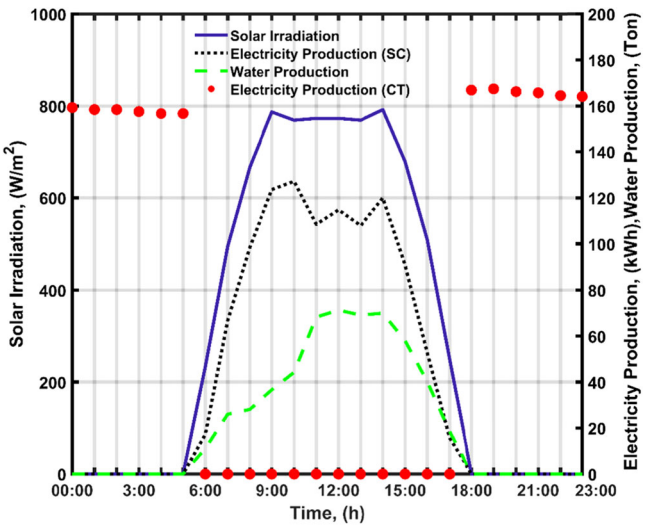

FIGURE 5 Solar irradiation, the electrical production for the solar chimney and the cooling tower, and the water production on 17th July in Qaisumah, Kingdom of Saudi Arabia

3.3 | Hourly average solar irradiation

Figure 6 investigates the distribution of the hourly average solar irradiation during the daytime over the entire year period for the five cities, representing five geographical areas. The lowest value of solar irradiation in all the data was 431.34 W/m^2, which was found in Turaif (north), in November. The highest value was 702.41 W/m^2 found in the city of Shahrurah (south), in January. Additionally, the lowest and highest values of solar irradiation for each month were highlighted. It was The highest solar irradiation values occurred in January, February, October, November, and December in Shahrurah (south). For the months of (March, April, and May) the highest solar irradiation value was observed to occur in Jeddah (west). Riyadh (center) had the highest solar irradiation value in June, and in Dhahran (east) the highest solar irradiation value was observed in the months of (July, August, and September). The lowest solar irradiation values belong to Turaif (north) during the months of (January, February, March, May, October, November, and December), Jeddah (west) for the months of (June and July), Riyadh (center) for the months of (August and September), and

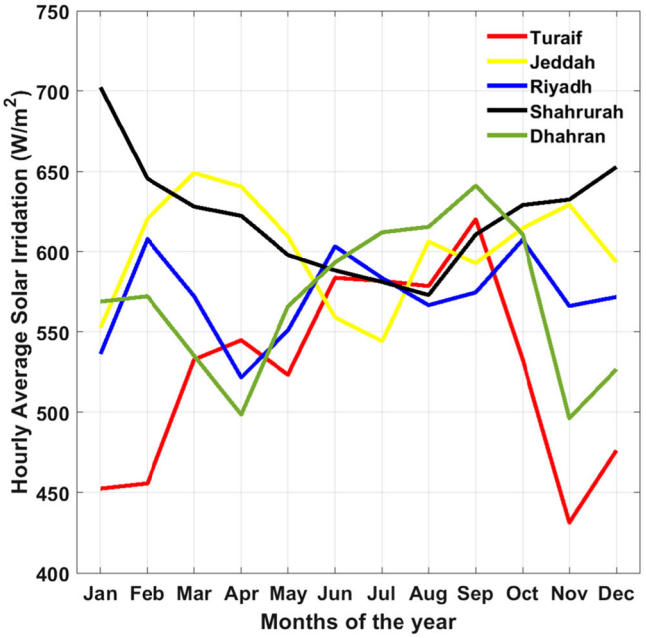

FIGURE 6 Hourly average solar Irradiation during the daytime for the cities (Turaif, Jeddah, Riyadh, Shahrurah, and Dhahran) for each month

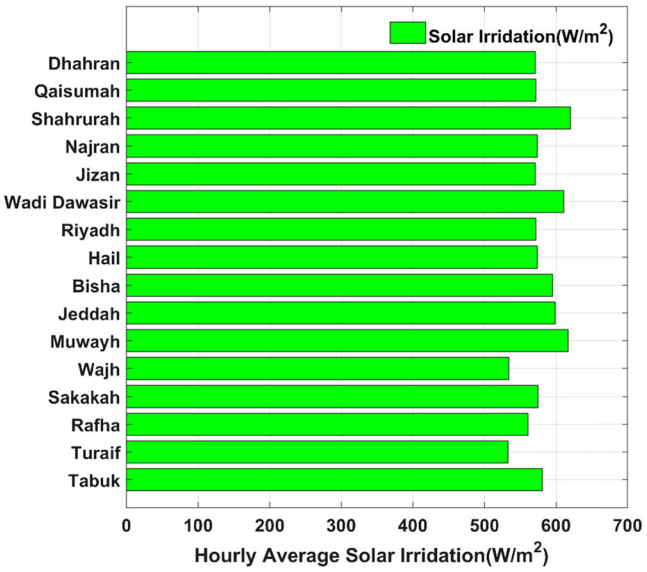

FIGURE 7 Hourly average solar irradiation for all selected cities over the year

Dhahran (east) for April. Turaif (north) had a large range of solar irradiation data between 431.34 W/m^2 in November and 620.15 W/m^2 in September. In contrast, Riyadh (center) had the smallest solar irradiation range between 521.68 W/m^2 in April and 607.94 W/m^2 in February. It can be observed that the five cities provided a clear representation of how the location plays a vital role in affecting solar irradiation, and consequently the productivity of the HSCCP (electrical energy and water production). Generally, from the trendlines in Figure 6, the differences between the values over the year seem to be the highest at the beginning and end of the year, however, in the middle of the year (May to September), the differences did not seem to be as much significant as in the other months. Meaning that fewer differences in solar irradiation values will be expected approximately in the specified period. It is anticipated that the productivity of the HSCCP for the cities located in the north will be the lowest they receive low solar irradiation all over the year. Turaif, which represents the north region of KSA, seemed to have the lowest solar irradiation values among other cities in most of the months of the year. On the other hand, the city of Shahrurah in the south recorded the highest solar irradiation values most of the year due to its location being closer to the equator. It should be said that the cities in one geographical area (north, south, etc.) will mostly have obvious variations in solar irradiation values because they are distributed over a large area (see Figure 3).

Figure 7 shows the comparison between the cities of KSA based on the hourly average solar irradiation values over the entire year. The highest value was found to be 620 W/m^2 for Shahrurah (south), while the lowest value was found to be 533 W/m^2 for Turaif (north). High solar irradiation values of 617 W/m^2 can be noticed in Muwayh (west), and 611 W/m^2 in Wadi Dawasir (center). On the other side, a low solar irradiation value of 534 W/m^2 was marked Wajh (west), and 561 W/m^2 in Rafha (north). As described before, one geographical area can have large differences in values of the main SCPP input operational parameters such as solar irradiation values. A good example of that can be observed in Figure 7, which presents the hourly average solar irradiation for all selected cities over the year. Within one geographical area (e.g., the west) two cities have the highest solar irradiation values (Muwayh and Jeddah) and one city (Wajh) with a low solar irradiation.

3.4 | Average ambient temperature

Figure 8 presents the average ambient temperatures for selected cities. The lowest and highest values for each month were highlighted. It was found that the highest ambient temperature values in January and February occurred in Jeddah (west). While the highest ambient temperature values in March and April, May occurred in Shahrurah (south). The months June, July, August, and September exhibited the highest ambient temperatures in Dhahran (east). It was observed that Jeddah (west) had the highest ambient temperature values in October,

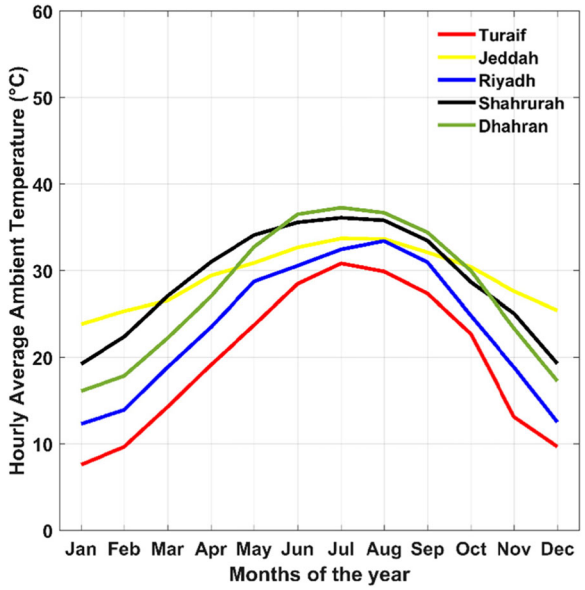

FIGURE 8 Hourly average ambient temperature for the cities (Turaif, Jeddah, Riyadh, Shahrurah, and Dhahran) for each month

November, and December). The lowest ambient temperatures were observed in Turaif (north) all over the year except January. On the other hand, Riyadh (center) had the lowest ambient temperature value. The largest temperature range was observed in Turaif (north) between 7.59°C and 30.8°C. Alternatively, Jeddah (west) had the smallest temperature range varying from 23.8°C to 33.7°C. Moreover, the highest value all over the available data was 37.3°C in July for Dhahran (east), and the lowest one was 7.59°C in January for Turaif (north). After considering the trends in Figure 8, it can be seen that the five cities have almost the same behavior, the lower ambient temperatures values are found to be at the beginning and end of the year and higher values are found to be at the middle of the year, however, the corresponding ambient temperatures trend differs from a city to another. For example, although Turaif (north) and Riyadh (center) have similar trend line styles, the temperatures that form their trend lines are much lower.

3.5 | The arrangement of the year timeline

As concluded from previous discussions, the time of the year greatly affects the weather conditions and solar irradiation in the different locations of KSA. Consequently, the electrical energy and water production values for each city can be dependent on the time of the year. To facilitate the analysis of the data the SCPP productivity was separated as per the weather data distribution all over the year in each city. Meaning that each period will include 3 months as described in Table 2. It was observed that wind speed over the year for all the cities had a different behavior than solar irradiation and temperature. Therefore, it was easier to be divided over a timeline rather than a geographical area.

TABLE 2 The division of the year timeline

Period No.	Months included
Period 1	January–February–March
Period 2	April–May–June
Period 3	July–August–September
Period 4	October–November–December

3.6 | Hourly average wind speed

The analysis of the hourly average wind speed data is essential as it is expected to affect water production, and hence, the HSCPP performance. In other words, higher wind speed will result in higher water production due to the increase in wind speed with the altitude of the chimney. Hence, the water production of the cities of concern should be correlated to the wind speed. The four upcoming figures present the hourly average wind speed values in the four periods.

Figure 9 shows that the highest wind speed values in period 1 were 4.82 (January), 5.53 (February), and 5.83 m/s (March), for the cities of Wadi Dawasir (center), and Riyadh (center). However, the lowest wind speed values were distributed over different cities of Muwayh (west), Bisha (west), and Najran (south), with values of 1.45, 1.58, and 2.07 m/s, respectively.

For period 2, Figure 10 shows that all the highest values of wind speed are found to be for the city of Riyadh (center) with values of 6.39 (April), 6.33 (May), and 5.85 m/s (June). The lowest wind speed value was found to be in April at 2.05 m/s in Najran (south), while the lowest wind speed values of May and June were owned by Muwayh (west) with values of 1.93 and 1.08 m/s, respectively.

In Figure 11, the values of wind speed of period 3 are represented. Interestingly, all the highest values belonged to Riyadh (center) with values in order of 5.12 (July), 4.44 (August), and 4.78 m/s (September). Also, the lowest value of July was 1.91 m/s for Bisha (west). The remaining lowest values were 1.01 (August) and 0.90 m/s (September), and they were owned by Muwayh (west).

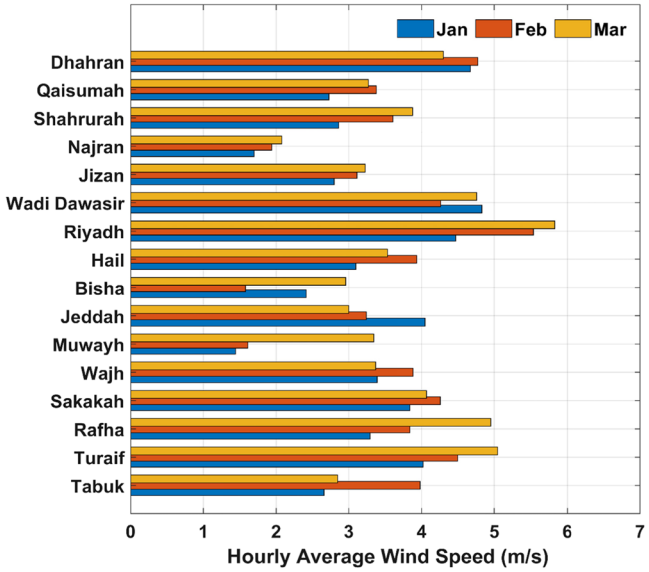

FIGURE 9 Hourly average wind speed (m/s) for (January–February–March) for all selected cities

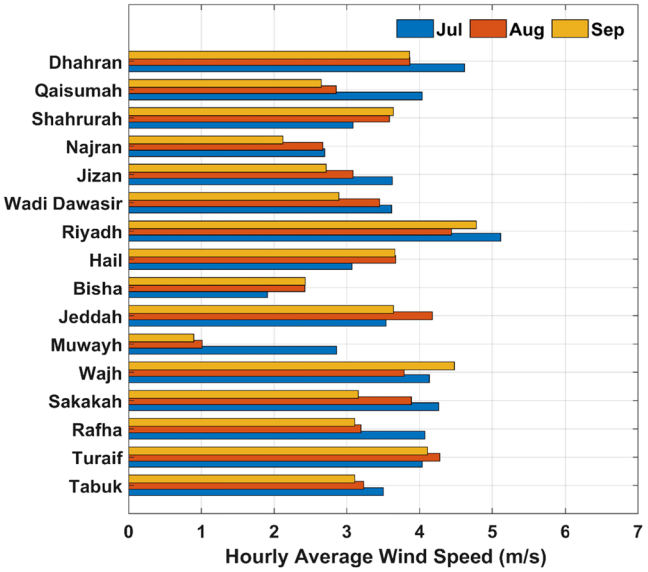

FIGURE 11 Hourly average wind speed (m/s) for (July–August–September) for all selected cities

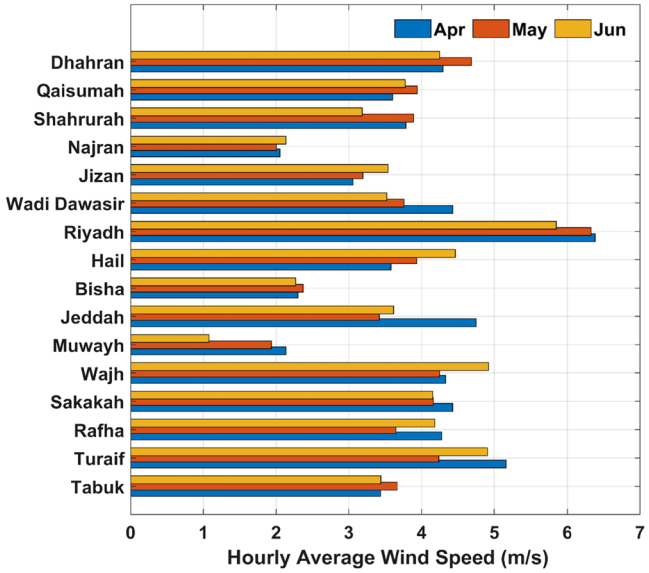

FIGURE 10 Hourly average wind speed (m/s) for (April–May-June) for all selected cities

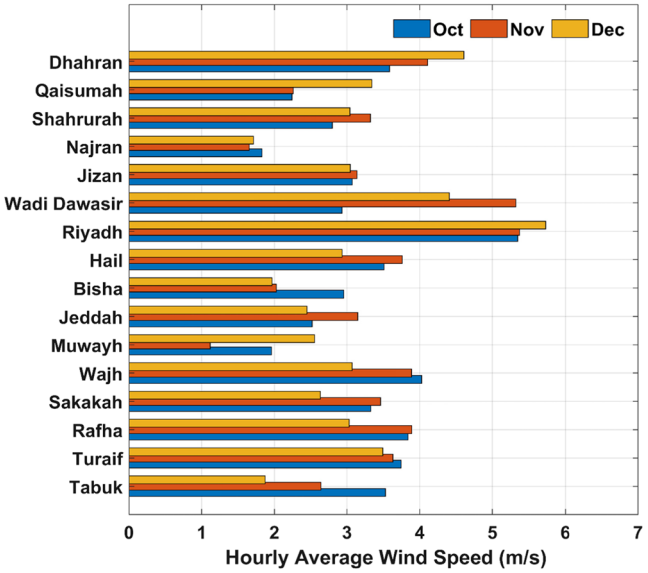

FIGURE 12 Hourly average wind speed (m/s) for (October–November–December) for all selected cities

For period 4, Figure 12, like periods 2 and 3, the highest values of wind speed were all for Riyadh (center) with values of 5.35 (October), 5.37 (November), and 5.73 m/s (December). Alternatively, the lowest values were found to be 1.83 m/s (October) for Narjan (south), 1.12m/s (November) for Muwayh (west), and 1.71 m/s (December) for Narjan (south).

Based on the presented figures, it can be concluded that Riyadh (center) had the lead in the highest wind speed values in almost all the months of the year, except January, where the highest value was for Wadi Dawasir (center). Other cities with high wind speed values that should be mentioned are Turaif (north), Wajh (west), and Dhahran (east). On the other hand, the lowest values of wind speed belonged to the cities of Muwayh (west), Bisha (west), and Najran (south). Table 3 shows the summary of the cities with the highest and the lowest wind speed values.

As a result, it can be said that the distribution of wind speed over cities of KSA is different from the pattern found for the distribution of the temperature or the solar irradiation, where the highest values were nearer to the

TABLE 3 Summary of the cities with the highest and the lowest wind speed

	Highest value location	Lowest value location
Period 1	Riyadh (center)	Muwayh (west)
Period 2	Riyadh (center)	Muwayh (west)
Period 3	Riyadh (center)	Muwayh (west)
Period 4	Riyadh (center)	Muwayh (west)

south and the lowest values were nearer to the north. Consequently, the wind speed should be taken into consideration while analyzing the production values, especially, the water production ones.

Additionally, it should be said that the cities with high wind speed values such as Riyadh (center) and Wadi Dawasir (center) are expected to have high water production values because it will speed up the water condensation, if the other parameters of interest such as solar irradiation, and ambient temperature were favored. However, if the other parameters are not meeting the requirements, low values of water production will be expected. For example, Turaif (north) had a considerable high value for wind speed, yet, it had very low values of solar irradiation and temperature, so it cannot be expected to have high values of water production.

3.7 | Energy and water productions

3.7.1 | Energy productions

As can be seen from Figure 13, the values of the electrical energy production vary between 600.7 kWh in January in Turaif (north) and 1525.9 kWh in March in Shahrurah (south). Remarkably, the lowest value of electrical energy production in each of the 3 months (January, February, and March) addressed in the figure was observed in the city of Turaif (north) and the highest one belonged to Shahrurah (south). For instance, in January, the lowest value was 600.7 kWh (Turaif) and the highest one was 1113.6 kWh (Shahrurah). One thing that should be pointed out is that most cities show an increase in electrical energy production values over time. By taking Narjan (south) as an example, the values recorded were 959.2, 1076.9, and 1167.6 kWh for January, February, and March, respectively. In addition, Wadi Dawasir (center), Bisha (west) recorded high values over period 1. These values were 1130.1 (February) and 1249.8 kWh (March) for Wadi Dawasir, and 991.7 kWh (January) for Bisha city. On the contrary, low values that should be highlighted are 765.6 kWh (January) for

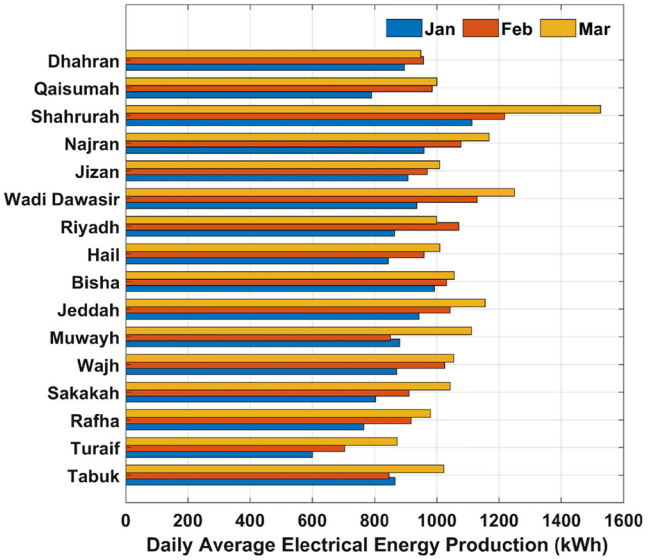

FIGURE 13 Daily average electrical energy production (kWh) for (January–February–March) for all selected cities

Rafha (north), 847.2 kWh (February) for Tabuk (north), and 948.8 kWh (March) for Dhahran (east).

Similarly, Figure 14 will proceed with representing the electrical energy production data focusing on period 2 (April, May, and June). The highest and the lowest values of period 2's entire data were in March with values of 946.3 kWh for Wajh (west) and 2782.1 kWh for Jizan (south). In January, 955.8 kWh was the lowest value belonged to Wajh (west) and the highest value was 1973.8 kWh for the city of Shahrurah (south). In May, the lowest value was 1049.2 kWh owned by the city of Turaif (north), and the highest value was 2431.3 kWh for Jizan (south). In June, the lowest value was 946.3 kWh for the city of Wajh (west) and 2782.1 kWh was the highest value for the city of Jizan (south). It can be noticed that values in period 2, where the highest value in it was slightly below the value of 3000 kWh, are much higher than in period 1, where the highest value is slightly above 1500 kWh. To put it in another way, a period of 3 months can greatly affect electrical energy production. Furthermore, a similar observation between period 1 and period 2 is that, as time passes in the consecutive months, the electrical energy production values increases in most of the cities presented.

As shown, the electrical energy production values over period 3 (July, August, and September) were illustrated in Figure 15. All the lowest values of electrical energy production in July (1140.0 kWh), August (1063.1 kWh), and September (738.2 kWh) belonged to the city of Wajh (west). On the contrary, the highest values of (2902.5 kWh) July, (2818.9 kWh) August, and, (2513.0 kWh) September were owned by Jizan (south),

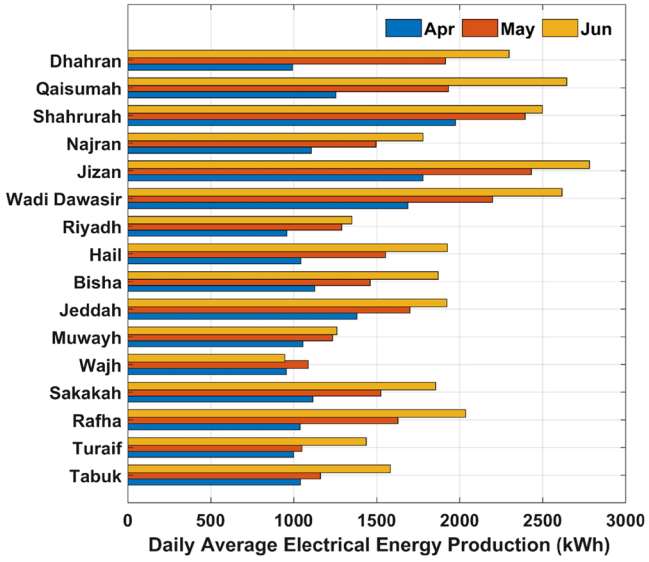

FIGURE 14 Daily average electrical energy production (kWh) for (April–May–June) for all selected cities

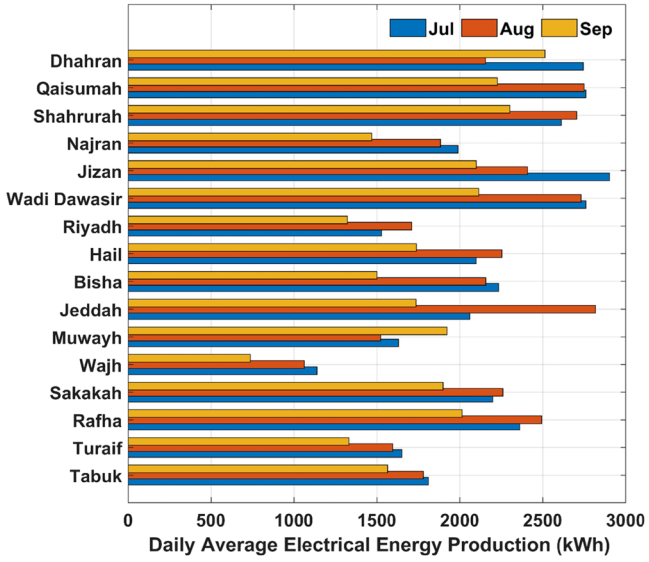

FIGURE 15 Daily average electrical energy production (kWh) for (July–August–September) for all selected cities

Jeddah (west), and Dhahran (east), respectively. Other high values that should be mentioned are 2761.4 kWh in July for Wadi Dawasir (center), 2750.2 kWh in August for Qaisumah (east), and 2301.3 kWh in September for Shahrurah (south). Also, low values that need to be mentioned are 1527.5 kWh for Riyadh (center) in July, 1522.4 kWh for Muwayh (west) in August, and 1323.8 kWh for Riyadh (center). One difference that needs to be mentioned is that, unlike the two previous periods, the values of the electrical energy production in

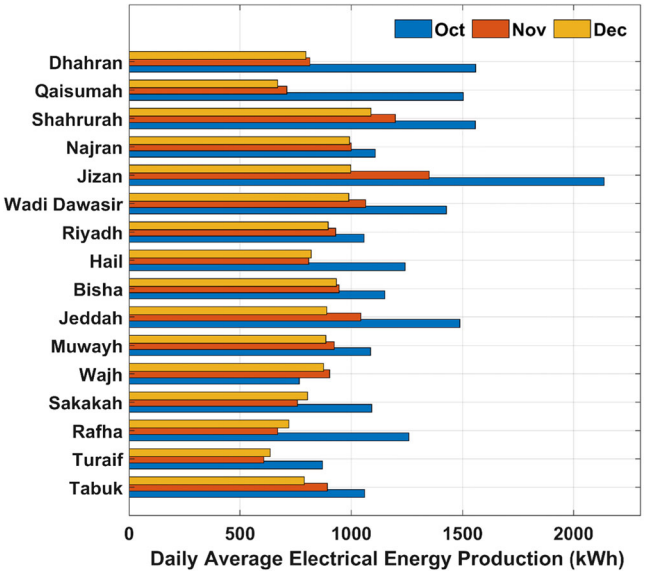

FIGURE 16 Daily average electrical energy production (kWh) for (October–November–December) for all selected cities

period 3 tend to decrease over time in the majority of the available cities.

Next, the electrical energy production values of period 4 are represented in Figure 16. The highest value in all data was 2137.7 kWh in Jizan (south) and it is the highest value for October, as well. In contrast, the lowest value found in all data was 606.3 kWh in Turaif (north) and it was the lowest value in November. In December, the lowest value was 653.3kWh for the city of Turaif (south) and the highest value was 1087.4 kWh for the city of Shahrurah (south). The other high values that should be mentioned are 1559.1 kWh in October for Dhahran, 1197.1 kWh in November for Shahrurah, and 997.6 kWh in December for Jizan city. Moreover, other low values were found to be 870.4 kWh in October for the city of Turaif (north), 668.8 kWh in November for the city of Rafha (north), and 668.3 kWh in December for the city of Qaisumah (east). Like period 3, the data of period 4 seems to decrease over time.

As can be seen from the previous discussion, the cities located in the south provided the highest values of electrical energy production over the year. On the contrary, the cities located in the north and some of the cities located in the west gave the lowest values of electrical energy production. That is because the cities located in the south are receiving the highest solar irradiation and have high temperatures among the rest of the cities. However, the cities in the north and the west are receiving lower solar irradiation and have lower temperatures. Interestingly, the remaining cities varied in their electrical energy production values. In other words, the cities that are closer to the south area seemed to give higher values than the ones close to the north area.

Another important aspect to discuss is that the values of electrical energy production had the same pattern in almost all the cities over the year, which was an increase over time in values in period 1 and period 2 and a decrease in values in period 3 and period 4. This can be justified in twofolds one related to the electrical energy production from the CT and the other is related to the electrical energy production from the SC. First, the CT performance is dependent on weather conditions, mainly air humidity and temperature. Additionally, when the outside air is dry and hot, less water spray will be needed to cool the dry air, hence less energy consumed to spray the water. As a result, the weather conditions in the early months of the year and the last months of the year, which have air with low temperature and high humidity, are not favorable for the performance of the CT. Second, the SC performance is not only affected by solar irradiation during the daytime. The temperature is one of the important aspects that have a direct impact on the electrical energy production from the SC because the temperature difference between the air under the collector and the ambient air affects the velocity of the air moving up, and when this temperature gradient is high, the velocity will be higher, giving more output for the turbine producing more electrical energy. This temperature gradient will be the highest in the months where the ambient air is hot, mainly months in period 2 and period 3. Table 4 summarizes the highest and lowest electrical energy productions based on the location and time of the year.

The annual power generation from the HSCPP can be seen to be significant. The total annual electricity production reported in this study is 2.5–3 times greater than the traditional SCPP (377 MWh) reported by Tavakolinia[62] and 1.9–2.3 orders of magnitude higher than HSCPP (528 MWh) in Jordan as reported by Abdelsalam et. al.[40] Furthermore, the power generation reported in this study is significantly greater than the values reported in the literature under comparable climate conditions. Tingzhem et al.[67] reported only 35 kW from SCPP operated under solar radiation intensity of 800 W/m^2. Larbi et al.[68] generated 140–200 kW under solar irradiation and ambient temperature in the range of 400–600 W/m^2 and 20°C–38°C, respectively. Abdelmohimen et al.[40] showed a SCPP with no more than 55–63 kW under solar irradiation in the range of 715–765 W/m^2.

3.8 | Water productions

Similarly, for clearer data analysis the water production data need to be represented in the format of dividing the year into four periods. In Figure 17, the water production data for period 1 is illustrated. As can be seen, in January, the highest value was found to be 348.8 tons for Dhahran (south), and the lowest value was 158.4 tons for Muwayh (west). In February, the lowest value was for Muwayh (west) with a value of 166.1 tons, and the highest value was 411.1 tons owned by Riyadh (center). In March, 428.5 tons was the highest value owned by Wadi Dawasir (center), and 267.7 tons was the lowest value identified for Najran (south). It should be said that, in period 1, the values of water production in most of the cities increased over time.

In Figure 18, the distribution of water production values for period 2 is shown. In April, the highest value was 474.0 tons for Jeddah (west), and the lowest value was 213.5 tons for Najran (south). In May and June, the highest values were 457.5 and 472.7 tons, respectively, for Dhahran (east). In addition, the lowest values for May and June were 232.5 and 159.2 tons, respectively, which belonged to Muwayh (west). Unlike period 1, the sequences of values of water productions in period 2

TABLE 4 Summary of the cities with the highest and the lowest electrical energy production

	Highest value location	Lowest value location
Period 1	Shahrurah (south)	Turaif (north)
Period 2	Jizan (south)	Wajh (west)
Period 3	Jizan (south)	Wajh (west)
Period 4	Jizan (south)	Turaif (north)

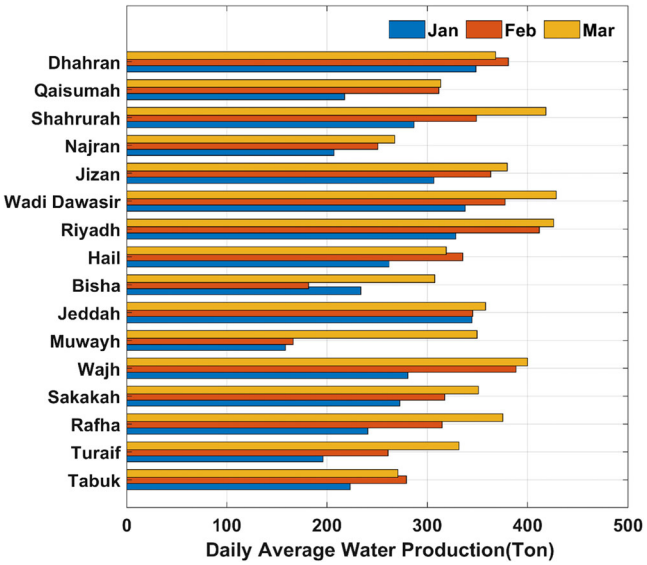

FIGURE 17 Daily average water production (ton) for (January–February–March) for all selected cities

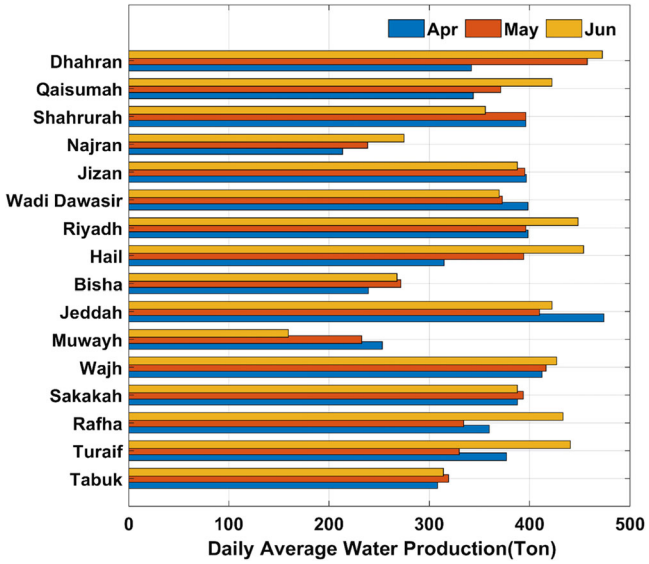

FIGURE 18 Daily average water production (ton) from April to June for all selected cities

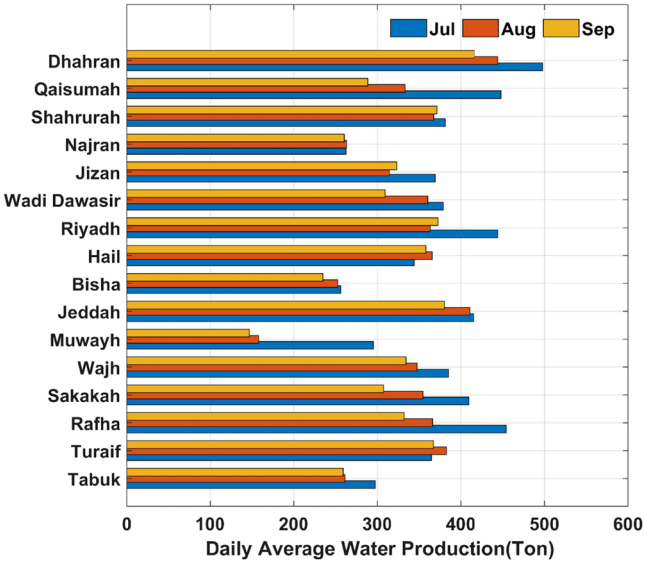

FIGURE 19 Daily average water production (ton) from July to September for all selected cities

seemed to differ between the cities. In other words, some cities had a pattern of increase over time, others had a decreasing pattern, and others had a nonconsistent pattern.

As can be seen, the period 3 data of water production were illustrated in Figure 19. Surprisingly, all the highest values of July, August, and September were for Dhahran (east), with the values of 497.7, 444.2, and 416.4 tons, respectively. However, the lowest values of period 3 were distributed in two cities: Bisha (west) had the lowest value in July, which was 256.1 tons, and Muwayh (west) had the remaining lowest values in August, and September with values of 158.3 and 147.1 tons, respectively. There is a common factor found between period 1 and period 3, which is that many of the cities follow the same pattern. However, unlike period 1, period 3 values seemed to decrease over time in most of the cities.

In Figure 20, the allocation of period 4 data of water production is demonstrated, where the values of concern are distributed in different cities. The highest value of October was Riyadh (center) with a value of 441.7 tons. For Wadi Dawasir (center), it owned the highest value in November, which was 415.5 tons. For Jizan (south), it had the highest value of December, which was 364.6 tons. In October, the lowest value was 256.3 tons for Muwayh (west). In November, the lowest value was 146.0 tons for Qaisumah (east). In December, 161.6 tons was the lowest value, which belonged to Tabuk (north). In period 4, the sequences of the values of water production seemed to be like period 2, meaning that it was not possible to generalize one pattern for all

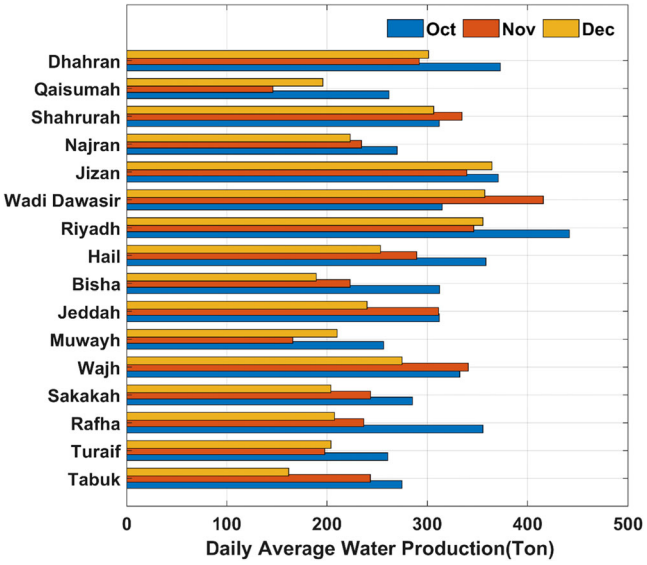

FIGURE 20 Daily average water production (ton) from October to December for all selected cities

cities, as some of the cities had values that seemed to decrease over time, and other cities had variations in values.

It can be concluded from the previous discussion that the water production values pattern greatly differs from the electrical energy production values pattern. Because generalizing a similar behavior for cities in one geographical area was unachievable. Furthermore, the available data showed that the cities with the highest electrical energy production did not necessarily have the highest water production. For

instance, the southern cities of Shahrurah, Najran, and Jizan recorded most of the highest values of electrical energy production. However, their water production values were not considered high, and they even owned the lowest values for some months. As a result, there should be parameters other than the solar irradiation, and the temperature, that participates cohesively with these parameters to influence the water production of each city. One of these potential parameters could be wind speed.

As expected, before the wind speed discussion, Riyadh (center), Wadi Dawasi (center), and Dhahran (east) had considerable high-water productions because of the positive participation of their high wind speed values, while having favorable solar irradiation and temperature values. As expected, although, Turaif (north), and had apparent high values of wind speed, it did not give high water production values because of its location in the north which is characterized by low solar irradiation and low temperature. Interestingly, Jeddah (west), which had moderate values of wind speed, stood out among the cities in period 2 with the highest value of water production. This emphasizes, even more, the fact that one parameter cannot be considered the only reason for any production value found. Alternatively, it is a combination of parameters that affect the performance of the power plant. Table 5 shows a summary of the highest and lowest water productions based on the location and time of the year.

It should be noted that several factors can impact the turbine during the HSCPP operation. The condensation of water and brine residual might have a negative impact on the performance of the turbine and the corresponding service life. This might cause corrosion problems among other operational issues. Similarly, water condensation could also happen on the collector roof. These issues were considered during the selection of the material for the construction of the HSCPP. The designer should consider these factors during their design. Furthermore, from a practical standpoint, regular maintenance is required to ensure the proper operation of the system.

TABLE 5 Summary of the cities with the highest and the lowest water production

	Highest value location	Lowest value location
Period 1	Wadi Dawasir (center)	Muwayh (west)
Period 2	Jeddah (west)	Muwayh (west)
Period 3	Dhahran (east)	Muwayh (west)
Period 4	Riyadh (center)	Qaisumah (east)

3.9 | Summary of annual results

Analyzing the data in Table 6 would allow the differentiation between the cities of concern on an annual scale. The city with the highest solar irradiation was Shahrurah, which is in the south. Not only that, Shahrurah had the lead in the electrical energy production in both the SCPP and HSCPP. However, the highest desalinated water production was found to belong to the city of Riyadh, which is in the center. The lowest solar irradiation found was for the city of Turaif, which is in the north. Additionally, the lowest electrical energy production for both SCPP and HSCPP modes was for Wajh, which is in the west. For the desalinated water production, Qaisumah, which is in the east, had the lowest value recorded. To conclude, the cities of Shahrurah (south) and Riyadh (center) are considered to have the highest values recorded, meaning that the application of HSCPP in the country of KSA will show the best results, if applicable, in these areas depending on the specific objectives required. Additionally, the cities of Wadi Dawasir (center), Dhahran (east), and Jizan (south) showed very promising results that cannot be neglected. The cities with high performance mentioned are marked in the following map, Figure 21.

3.10 | Environmental impact assessment

Reflecting on the application of the HSCPP can be very beneficial in aspects related to the environment. Producing clean energy and reducing CO_2 emissions are the most significant ones. Calculating the reduction in CO_2 emissions can be done based on the fact that the amount of CO_2 emissions caused by a coal-fired plant is estimated to be 0.95 kg CO_2 eq./kWh of electricity.[56] Consequently, reduction of CO_2 emissions can be found by:

$$CO_2\text{mass(kg)} = 0.95 \times \text{production of electrical energy (kWh)}.$$

A representation of the annual electric power production, freshwater production, and the annual reduction of CO_2 emissions for conventional SCPP and HSCPP can be found in Table 7. The data available for the hybrid system is based on Qaisumah in KSA. By comparison between the two modes, the hybrid mode gives higher electrical power production by almost 55% and higher freshwater production by almost 20%. Additionally, there is an obvious increase in the CO_2 emissions reduction by approximately 56%. The results

	Solar irradiation (kWh/m^2)	Solar chimney power plant (MWh/year)	Hybrid solar chimney power plant (MWh/year)	Desalinated water (ton/year)
Bisha	2447	353.42	501.65	90,542
Jeddah	2453	371.64	554.4	134,463
Muwayh	2501	351.31	437.64	77,868
Wajh	2168	317.57	347.59	131,832
Qaisumah	2311	342.89	586.2	11,109
Dhahran	2334	356.02	566.8	142,843
Rafha	2274	343.56	514.72	122,009
Sakakah	2339	352.39	495.77	119,065
Tabuk	2377	348.12	439.38	97,610
Turaif	2100	320.59	376.52	112,938
Hail	2334	354.31	496.78	123,068
Wadi Dawasir	2516	380.7	637.31	134,420
Riyadh	2321	351.16	425.55	143,898
Najran	2368	345.04	488.2	90,215
Jizan	2343	353.52	664.16	131,106
Shahrurah	2583	393.17	676.20	130,021

TABLE 6 Annual electrical energy production and desalinated water production

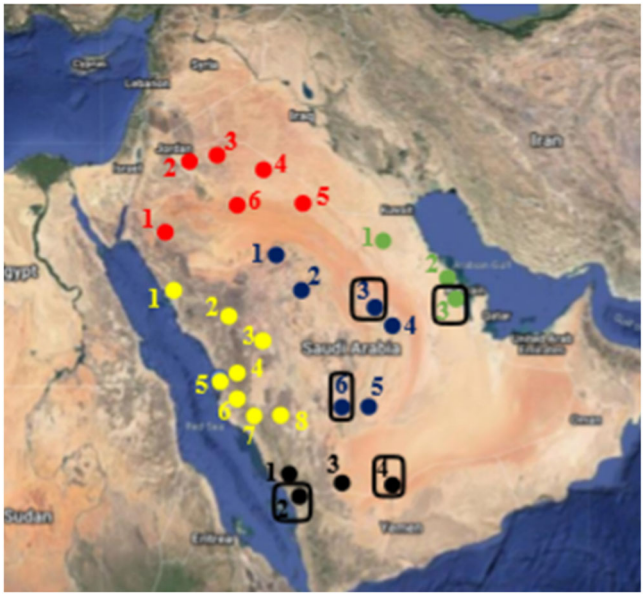

FIGURE 21 Kingdom of Saudi Arabia map with potential cities for the application of hybrid solar chimney power plant. (Two in black is Jizan city, four in black is Shahrurah, six in blue is Wadi Dawasir, three in blue is Riyadh, and three in green is Dhahran)

illustrated show the ability of the proposed design of being sustainable and reliable with additional Electrical power and freshwater production and less CO_2 emissions.

TABLE 7 Performance comparison between traditional solar chimney power plant (SCPP) and hybrid solar chimney power plant (HSCPP)

Item	SCPP[57]	HSCPP
Electrical power production, (kWh/year)	377,000	586,208
Freshwater production (metric tons/year)	92,616	111,095
CO_2 emission reduction (tons/year)	358	556.9

4 | CONCLUSION

This study shows the feasibility of deploying the HSCPP in 16 several cities, that span the entire geographical area of the KSA. Although the performance of the HSCPP in terms of electricity production and water production differs from one city to another, all cities, in general, showed good performances compared to traditional SCPP. The results also revealed that the HSCPP outperformed the traditional SCPP by a factor of two in terms of electricity and freshwater generated, as well as CO_2 reduction. The proposed HSCPP generates annual electrical energy and desalinated water in the range of 376.52–676.20 MWh and 77,868–143,898 tons in all the studied cities. Although the HSCPP would be a

viable solution for supplying electricity and clean water, future research could look into connecting the HSCPP to other renewable energy harvesting systems. Furthermore, consideration should be given to the sustainability of the structure over a long period, by performing regularly scheduled maintenance for the turbine, sprinkles, and removal of the silt deposits due to the seawater pool. Future work will focus on improving the design structure with flexible configurations and introducing artificial intelligence to select the optimal operating mode (CT mode or SCPP mode) based on forecasted weather data.

ACKNOWLEDGMENT

Special thanks to Asma Khasawneh for helping with the diagrams.

ORCID

Fares Almomani http://orcid.org/0000-0003-4785-4567

REFERENCES

1. Motschmann A, Teutsch C, Huggel C, et al. Current and future water balance for coupled human-natural systems–insights from a glacierized catchment in Peru. *J Hydrol Region Stud*. 2022;41:101063.
2. Ağbulut Ü. Forecasting of transportation-related energy demand and CO_2 emissions in Turkey with different machine learning algorithms. *Sustain Prod Consumpt*. 2022;29:141-157.
3. Almomani F, Al Ketife A, Judd S, et al. Impact of CO_2 concentration and ambient conditions on microalgal growth and nutrient removal from wastewater by a photobioreactor. *Sci Total Environ*. 2019;662:662-671.
4. Judd SJ, Al Momani FAO, Znad H, Al Ketife AMD. The cost benefit of algal technology for combined CO_2 mitigation and nutrient abatement. *Renew Sustain Energy Rev*. 2017;71:379-387.
5. Alami AH, Abu Hawili A, Tawalbeh M, et al. Materials and logistics for carbon dioxide capture, storage and utilization. *Sci Total Environ*. 2020;717:137221.
6. Al Ketife AMD, Almomani F, EL-Naas M, Judd S. A technoeconomic assessment of microalgal culture technology implementation for combined wastewater treatment and CO_2 mitigation in the Arabian Gulf. *Process Saf Environ Prot*. 2019;127:90-102.
7. Almomani F, Judd S, Bhosale RR, Shurair M, Aljamal K, Khraisheh M. Intergraded wastewater treatment and carbon bio-fixation from flue gases using Spirulina platensis and mixed algal culture. *Process Saf Environ Prot*. 2019;124:124-250.
8. Gross R, Leach M, Bauen A. Progress in renewable energy. *Environ Int*. 2003;29(1):105-122.
9. Nematollahi O, Hoghooghi H, Rasti M, Sedaghat A. Energy demands and renewable energy resources in the Middle East. *Renew Sustain Energy Rev*. 2016;54:1172-1181.
10. Ahmadi MH, Ghazvini M, Sadeghzadeh M, et al. Solar power technology for electricity generation: a critical review. *Energy Sci Eng*. 2018;6(5):340-361.
11. Gielen D, Boshell F, Saygin D, Bazilian MD, Wagner N, Gorini R. The role of renewable energy in the global energy transformation. *Energy Strategy Rev*. 2019;24:38-50.
12. Salameh T, Ghenai C, Merabet A, Alkasrawi M. Techno-economical optimization of an integrated stand-alone hybrid solar PV tracking and diesel generator power system in Khorfakkan, United Arab Emirates. *Energy*. 2020;190:116475.
13. Ellabban O, Abu-Rub H, Blaabjerg F. Renewable energy resources: current status, future prospects and their enabling technology. *Renew Sustain Energy Rev*. 2014;39:748-764.
14. Meckling J, Nahm J. The politics of technology bans: industrial policy competition and green goals for the auto industry. *Energy Policy*. 2019;126:470-479.
15. Almomani F, Bhosale RR, Kumar A, The Effect of Intermediate Ozonation Process on Improving Biogas Production from Co-digestion of Agricultural Waste and Manure. *TechConnect Briefs*; 2016.
16. Infield D, Freris L. *Renewable Energy in Power Systems*. John Wiley & Sons; 2020.
17. Panwar N, Kaushik S, Kothari S. Role of renewable energy sources in environmental protection: a review. *Renew Sustain Energy Rev*. 2011;15(3):1513-1524.
18. Al-Waeli AHA, Sopian K, Kazem HA, Chaichan MT. Photovoltaic/thermal (PV/T) systems: Status and future prospects. *Renew Sustain Energy Rev*. 2017;77:109-130.
19. Rofiqul Islam M, Rabiul Islam M, Rafiqul Alam Beg M. Renewable energy resources and technologies practice in Bangladesh. *Renew Sustain Energy Rev*. 2008;12(2):299-343.
20. Rourke FO, Boyle F, Reynolds A. Renewable energy resources and technologies applicable to Ireland. *Renew Sustain Energy Rev*. 2009;13(8):1975-1984.
21. Al-Smairan M, Shawaqfah M, AlMomani F. Techno-economic investigation of an integrated boiler–solar water heating/cooling system: a case study. *Energies*. 2020;14(1):1.
22. Schlaich J. *The Solar Chimney: Electricity from the Sun*. Axel Menges; 1981.
23. Schlaich J, Bergermann R, Schiel W, Weinrebe G. Sustainable electricity generation with solar updraft towers. *Int Assoc Bridge Struct Eng Eth-Honggerberg*. 2004;14:225-229.
24. Jing H, Chen Z, Li A. Experimental study of the prediction of the ventilation flow rate through solar chimney with large gap-to-height ratios. *Build Environ*. 2015;89:150-159.
25. Saifi N, Settou N, Dokkar B, Negrou B, Chennouf N. Experimental study and simulation of airflow in solar chimneys. *Energy Procedia*. 2012;18:1289-1298.
26. Kasaeian A, Ghalamchi M, Ghalamchi M. Simulation and optimization of geometric parameters of a solar chimney in Tehran. *Energy Convers Manage*. 2014;83:28-34.
27. Sangi R, Amidpour M, Hosseinizadeh B. Modeling and numerical simulation of solar chimney power plants. *Sol Energy*. 2011;85(5):829-838.
28. Pretorius JP, Kröger DG. Critical evaluation of solar chimney power plant performance. *Sol Energy*. 2006;80(5):535-544.

29. Fasel HF, Meng F, Shams E, Gross A. CFD analysis for solar chimney power plants. *Sol Energy*. 2013;98:12-22.
30. Pastohr H, Kornadt O, Gürlebeck K. Numerical and analytical calculations of the temperature and flow field in the upwind power plant. *Int J Energy Res*. 2004;28(6):495-510.
31. Zhou X, Wang F, Ochieng RM. A review of solar chimney power technology. *Renew Sustain Energy Rev*. 2010;14(8): 2315-2338.
32. Fathi N, McDaniel P, Aleyasin SS, et al. Efficiency enhancement of solar chimney power plant by use of waste heat from nuclear power plant. *J Clean Prod*. 2018;180:407-416.
33. Maia CB, Ferreira AG, Valle RM, Cortez MFB. Theoretical evaluation of the influence of geometric parameters and materials on the behavior of the airflow in a solar chimney. *Comput Fluids*. 2009;38(3):625-636.
34. Mathur J, Mathur S. Summer-performance of inclined roof solar chimney for natural ventilation. *Energy Build*. 2006;38(10):1156-1163.
35. Ming T, de Richter RK, Meng F, Pan Y, Liu W. Chimney shape numerical study for solar chimney power generating systems. *Int J Energy Res*. 2013;37(4):310-322.
36. Larbi S, Bouhdjar A, Chergui T. Performance analysis of a solar chimney power plant in the southwestern region of Algeria. *Renew Sustain Energy Rev*. 2010;14(1):470-477.
37. Guo P, Li J, Wang Y, Wang Y. Numerical study on the performance of a solar chimney power plant. *Energy Convers Manage*. 2015;105(2):197-205.
38. Pasumarthi N, Sherif S. Experimental and theoretical performance of a demonstration solar chimney model—part I: mathematical model development. *Int J Energy Res*. 1998;22(3):277-288.
39. Kiwan S, Salam QIA. Solar chimney power-water distillation plant (SCPWDP). *Desalination*. 2018;445:105-114.
40. Abdelmohimen MAH, Algarni SA. Numerical investigation of solar chimney power plants performance for Saudi Arabia weather conditions. *Sustain Cities Soc*. 2018;38:1-8.
41. Chergui T, Larbi S, Bouhdjar A. Thermo-hydrodynamic aspect analysis of flows in solar chimney power plants—a case study. *Renew Sustain Energy Rev*. 2010;14(5):1410-1418.
42. Xu Y, Zhou X. Performance of a modified solar chimney power plant for power generation and vegetation. *Energy*. 2019;171:502-509.
43. Khan MA, Rehman S, Al-Sulaiman FA. A hybrid renewable energy system as a potential energy source for water desalination using reverse osmosis: a review. *Renew Sustain Energy Rev*. 2018;97:456-477.
44. Zuo L, Ding L, Chen J, Zhou X, Xu B, Liu Z. Comprehensive study of wind supercharged solar chimney power plant combined with seawater desalination. *Sol Energy*. 2018;166:59-70.
45. Kiwan S, Al-Nimr Md, Salim I. A hybrid solar chimney/ photovoltaic thermal system for direct electric power production and water distillation. *Sustain Energy Technol Assess*.2020;38(2019):100680.
46. Abdelsalam E, Almomani F, Kafiah F, et al. A new sustainable and novel hybrid solar chimney power plant design for power generation and seawater desalination. *Sustainability*. 2021;13(21):12100.
47. Asnaghi A, Ladjevardi SM. Solar chimney power plant performance in Iran. *Renew Sustain Energy Rev*. 2012;16(5): 3383-3390.
48. Harris DJ, Helwig N. Solar chimney and building ventilation. *Appl Energy*. 2007;84(2):135-146.
49. Zandian A, Ashjaee M. The thermal efficiency improvement of a steam Rankine cycle by innovative design of a hybrid cooling tower and a solar chimney concept. *Renew Energy*. 2013;51:465-473.
50. Arce J, Jiménez MJ, Guzmán JD, Heras MR, Alvarez G, Xamán J. Experimental study for natural ventilation on a solar chimney. *Renew Energy*. 2009;34(12):2928-2934.
51. Afonso C, Oliveira A. Solar chimneys: simulation and experiment. *Energy Build*. 2000;32(1):71-79.
52. Fluri TP, Von TW. Backström, Performance analysis of the power conversion unit of a solar chimney power plant. *Sol Energy*. 2008;82(11):999-1008.
53. Miqdam TC, Hussein AK. Basement kind effects on air temperature of a solar chimney in Baghdad-Iraq weather. *Int J Appl Sci*. 2011;2(2):12-20.
54. Liu Q, Cao F, Liu Y, et al., Design and simulation of a solar chimney PV/T power plant in Northwest China. *Int J Photoenergy*; 2018.
55. Ninic N. Available energy of the air in solar chimneys and the possibility of its ground-level concentration. *Sol. Energy*. 2006;80(7):804-811.
56. Koonsrisuk A. Mathematical modeling of sloped solar chimney power plants. *Energy*. 2012;47(1):582-589.
57. Chantawong P, Hirunlabh J, Zeghmati B, Khedari J, Teekasap S, Win MM. Investigation on thermal performance of glazed solar chimney walls. *Sol Energy*. 2006;80(3):288-297.
58. Klimes L, Charvát P, Hejčík J. Comparison of the energy conversion efficiency of a solar chimney and a solar PV-powered fan for ventilation applications. *Energies*. 2018; 11(4):912.
59. Kommalapati R, et al., *Review of the Life Cycle Greenhouse Gas Emissions from Different Photovoltaic and Concentrating Solar Power Electricity Generation Systems*; 2017.
60. Kiwan S, Al-nimr M, Salim I. A hybrid solar chimney/ photovoltaic thermal system for direct electric power production and water distillation. *Sustain Energy Technol Assessm*. 2020;38(2019):100680.
61. Zuo L, Yuan Y, Li Z, Zheng Y. Experimental research on solar chimneys integrated with seawater desalination under practical weather condition. *Desalination*. 2012;298:22-33.
62. Tavakolinia F. *Wind-Chimney (Integrating the Principles of a Wind-Catcher and a Solar-Chimney to Provide Natural Ventilation)*; 2011.
63. Prima Y, Prima S. Wind catcher and solar chimney integrated as an alternative ventilation for urban dense settlements in tropical climate. *Int J Architect Urban*. 2019;3(1):51-68.
64. Ming T, Gong T, de Richter RK, Liu W, Koonsrisuk A. Freshwater generation from a solar chimney power plant. *Energy Convers Manage*. 2016;113:189-200.
65. Abdelsalam E, Kafiah F, Almomani F, et al. Performance analysis of hybrid solar chimney–power plant for power production and seawater desalination: a sustainable approach. *Int J Energy Res*. 2021;45:17327–17341.

66. Abdelsalam E, Kafiah F, Almomani F, et al. An innovative design of a solar double-chimney power plant for electricity generation. *Energies*. 2021;14(19):6235.
67. Tingzhen M, Wei L, Guoling X, et al. Numerical simulation of the solar chimney power plant systems coupled with turbine. *Renew Energy*. 2008;33:897-905.
68. Larbi S, Bouhdjar A, Meliani K, et al. *Solar Chimney Power Plant with Heat Storage System Performance Analysis in South Region of Algeria*; IEEE.

How to cite this article: Abdelsalam E, Almomani F, Ibrahim S. A novel hybrid solar chimney power plant: Performance analysis and deployment feasibility. *Energy Sci Eng*. 2022;10:3559-3579. doi:10.1002/ese3.1240